I&EC research
Industrial & Engineering Chemistry Research

Review

pubs.acs.org/IECR

Removal of Nanoparticles from Gas Streams by Fibrous Filters: A Review

Chiu-sen Wang*,† and Yoshio Otani‡

†Department of Public Health, National Taiwan University, Taipei 100, Taiwan

‡Graduate School of Natural Science and Technology, Kanazawa University, Kakuma, Kanazawa 920-1192, Japan

ABSTRACT: Although the basic principles of fibrous filters have been well understood for capture of micron and submicron sized particles, questions arise when they are applied to nanoscale particles. In the first part of this review, the classical theory of fibrous filters is described with focus on the principles that are applicable to nanoparticle collection. The areas of recent developments reviewed include thermal rebound of nanoparticles and the effects of particle shape, aggregate morphology, flow regime, humidity, fiber size, and particle loading. One of the outstanding questions in nanoparticle collection is the particle size at which the effect of thermal rebound on collection efficiency can be observed. Theoretical calculations indicate that the effect probably can be observed only for particles smaller than 1 nm, but experimental confirmation is difficult at present because of lack of instruments for classifying and counting subnanoscale particles. Two promising devices based on filtration principles have been studied in recent years: multilayer filters and inertial fibrous filters. Multilayer filters, which are composed of nanofiber and microfiber mats, have potential to become an efficient and economical device for removing nanoparticles from gas streams. The inertial fibrous filter operates at high flow rates and relatively low pressure drop, thereby offering an attractive alternative to low-pressure impactors for nanoparticle sampling. Further development of these two types of filtration devices is needed to make them simple and reliable.

INTRODUCTION

Particles smaller than 100 nm in at least one of their three external dimensions are referred to as nanoparticles or ultrafine particles. The term nanoparticle is primarily used to describe nanoscale particles manufactured for commercial, industrial, or medical applications, whereas ultrafine particle is a term traditionally used for nanometer-sized particles that are released into or formed in the atmosphere, such as particles in diesel exhaust, industrial fumes, and photochemical smog. Because of their unique properties, manufactured nanoparticles have many useful applications but also pose potential adverse effects on human health and the environment. Inhalation exposure to airborne nanoscale particles is a major health concern, as it can occur at home, in the workplace, and in the ambient environment. Epidemiological studies have found a higher incidence of chronic obstructive pulmonary disease, fibrosis, and lung cancer in workers exposed to certain types of nanoscale particles. There is an increasing body of scientific literature on the adverse health effects of inhaled nanoscale particles (see, for example, Borm and Kreyling,[1] Kreyling et al.,[2] Mills et al.,[3] and Oberdörster[4]), but the dosimetry and toxicology are still not well understood.

Fibrous filters are simple and economical devices capable of efficiently removing submicrometer particles from gas streams. Because fibers can be made of a wide variety of materials, such as cellulose, glass, plastics, ceramics, or metals, fibrous filters have been applied in many areas, including disposable respirators, industrial gas cleaning equipment, cleanroom air purification systems, automotive cabin air filters, and indoor air purifiers. They have also been employed to collect samples of aerosol particles for chemical analysis.

Although the basic principles of fibrous filters are well understood for capture of micron and submicron sized particles, a number of questions arise when they are applied to nanoparticle collection. One of these questions is the size of particles at which thermal rebound from fiber surfaces occurs and thereby deteriorates the filter performance. Another question relates to particle shape and aggregate morphology, which are distinct physical properties of nanoscale particles and appear to have marked effects on collection efficiency. In this review, the classical theory of fibrous filters is summarily described, with focus on the principles that are applicable to nanoparticle collection. The effects of various parameters including particle shape, aggregate morphology, flow regime, humidity, fiber size, and particle loading are discussed, and the needs for further studies on these parameters are suggested.

FILTRATION EFFICIENCY, PRESSURE DROP, AND THE MOST PENETRATING PARTICLE SIZE

A fibrous filter is made of a pad of loosely packed fibers which are generally perpendicular to the direction of aerosol flow. Collection efficiency and pressure drop are the parameters used to assess the performance of a filter. A good filter should have high collection efficiency and low pressure drop. At a given rate of aerosol flow, the collection efficiency is a function of particle size. The most penetrating particle size, defined as the particle

Special Issue: L. T. Fan Festschrift

Received: March 5, 2012
Revised: June 19, 2012
Accepted: June 28, 2012

dx.doi.org/10.1021/ie300574m | *Ind. Eng. Chem. Res.* XXXX, XXX, XXX–XXX

size for which a filter has the lowest collection efficiency, has also been adopted as a performance indicator. There is an extensive literature on the classical theory of fibrous filters (see, for example, Davies,[5] Brown,[6] Lee and Ramamurthi,[7] and Hinds[8]).

The collection efficiency is defined as the fraction of the entering particles that are collected by the filter

$$E = \frac{N_0 - N}{N_0} \quad (1)$$

where N_0 and N are, respectively, the particle number concentrations at the inlet and the outlet. Alternatively, mass concentration of particles can be used to define the efficiency.

For a high-efficiency filter, the penetration P $(= 1 - E)$ is a clearer indicator because it is a smaller number and therefore shows a larger relative change than does the collection efficiency. For instance, when E increases from 90 to 99%, P drops from 10 to 1%.

The volume fraction of fibers in a filter, known as the packing density or solidity (α), is an important parameter influencing the filter performance. Commercial fibrous filters typically have α values between 0.01 and 0.3. The flow velocity in a filter, U, is related to the face velocity (the flow velocity at the filter face), U_0, as follows

$$U = \frac{U_0}{1 - \alpha} \quad (2)$$

CAPTURE MECHANISMS

As an aerosol stream approaches a fiber, particles may deposit on the fiber by the simultaneous action of several mechanisms, including inertial impaction, interception, Brownian motion, gravitational settling, and electrostatic forces (Figures 1 and 2).

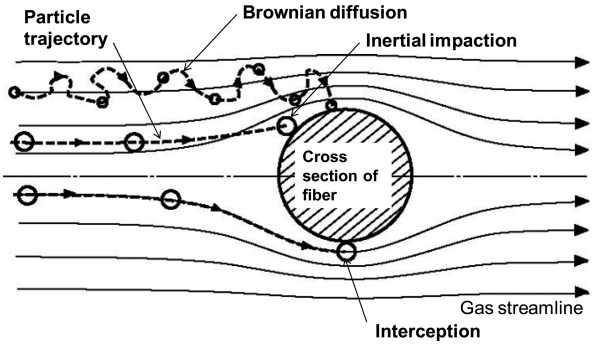

Figure 1. Particle collection by inertial impaction, interception, and convective Brownian diffusion.

The first four mechanisms do not depend on electrostatic forces and are known as mechanical capture mechanisms. Inertial impaction occurs when a particle, by its inertia, departs from the original gas streamline and hits a fiber. Interception takes place because a particle has a finite size, which leads to deposition when it comes within one particle radius of the fiber surface, even though it stays on the original streamline. For particles smaller than a few tenths of a micrometer, the Brownian motion can be sufficiently strong to move them from the original streamlines to a fiber. Gravitational settling can contribute to particle collection if the aerosol stream flows downward, but the contribution is negligible for nanoparticles.

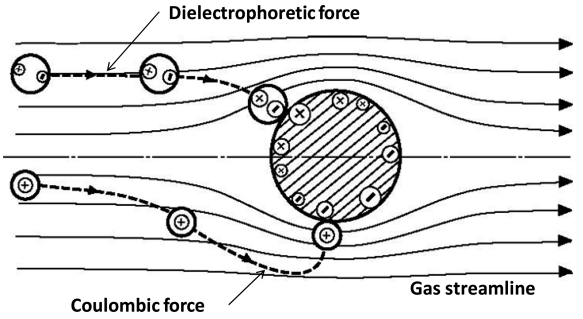

Figure 2. Particle collection by Coulombic and dielectrophoretic forces.

Electrostatic forces arise when particles or fibers carry electric charges or when an external electric field is applied to the filter. There are several types of electrostatic interactions.[9] Among them is the Coulombic force between a charged particle and a unipolar or bipolar charged fiber such as those in an electret filter. Another type of electrostatic interaction is the image force between a charged particle and a neutral fiber, as a result of polarization of the fiber by the particle charge. Similarly, a unipolar or bipolar charged fiber can polarize a neutral particle, thereby giving rise to dielectrophoretic forces on the particle. An externally applied electric field can polarize a fiber and the nonuniform field thus created around the fiber can move a charged particle toward the fiber. Polarization of particles by an externally applied electric field also can produce dielectrophoretic forces on them.

For nanoparticles, deposition on fibers takes place mainly by convective Brownian diffusion and interception. Inertial impaction, Coulombic forces, and dielectrophoretic forces may play important roles under certain conditions.

SINGLE FIBER EFFICIENCY

The classical theory of filtration is based on the concept of single fiber efficiency, defined as the ratio of the number of particles collected by a unit length of a clean fiber to the number of particles in the undisturbed mainstream (far upstream of the fiber) passing through the projected area of the fiber section under consideration (Figure 3). Making a mass balance for particles in an infinitesimal thickness of the filter and then integrating from the filter face to the exit gives

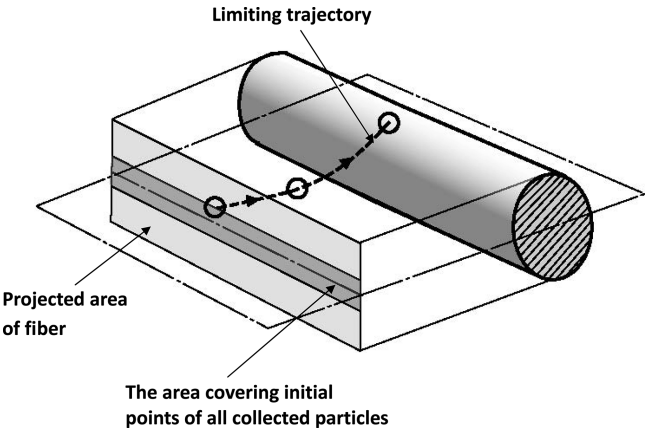

Figure 3. Definition of single fiber efficiency.

dx.doi.org/10.1021/ie300574m | Ind. Eng. Chem. Res. XXXX, XXX, XXX–XXX

$$E = 1 - \exp\left[\frac{-4\alpha\eta\, L}{\pi\, d_f(1-\alpha)}\right] \quad (3)$$

where η is the single fiber efficiency, L is the filter thickness, and d_f is the fiber diameter. Eq 3 is based on four assumptions: (1) the packing density is uniform throughout the filter, (2) all fibers are straight and have the same diameter, (3) all fibers are perpendicular to the flow direction, and (4) the single fiber efficiency remains unchanged along the depth of the filter. A real filter is unlikely to satisfy all these assumptions. The collection efficiency tends to be lower than estimated by eq 3 if the packing density is not uniform or not all fibers are perpendicular to the flow direction. Figure 4 illustrates

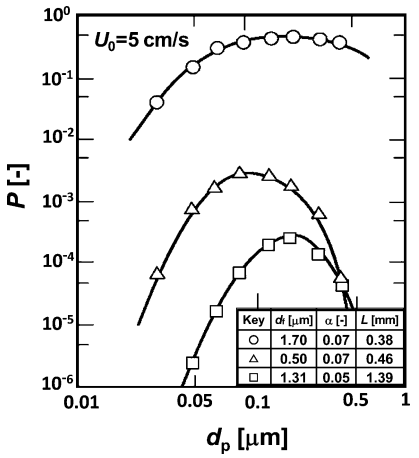

Figure 4. Penetration versus particle diameter for three sets of test conditions. The test particles were neutralized monodisperse NaCl particles, generated and classified using a Collison atomizer, a diffusion dryer, and a DMA. The penetration data were taken at room temperature and atmospheric pressure.

penetration through real filters as a function of particle size and other parameters. In practice, eq 3 has been used to calculate the effective single fiber efficiency of a filter from experimentally determined values of E, α, L, and average d_f.

The single fiber efficiency varies with particle property, filter structure, fiber property, flow rate, and electric field in a filter. Analysis of the single fiber efficiency constitutes the main part of the classical theory of fibrous filters. Theoretical analyses have been made for single fiber efficiencies due to individual capture mechanisms and due to interception acting together with another mechanism. To calculate the overall collection efficiency due to all mechanisms acting together, it is usually assumed that the efficiencies due to individual mechanisms (and two mechanisms acting together for which efficiency expressions have been derived) are additive. Such an approach tends to overestimate the overall efficiency, because the capture of a particle could be counted more than once. For the particle size range in which one capture mechanism predominates, it has been shown that the efficiency due to that mechanism alone gives a better estimate of the overall efficiency than does the sum of all individual mechanism efficiencies.

To derive the expressions for single fiber efficiency, the following two assumptions are commonly made: the fiber is clean and there is no particle rebound from the fiber. For capture by inertia impaction, interception, and electrostatic forces, the single fiber efficiency can be calculated from the equation of particle motion using the concept of limiting trajectory, which is defined as the trajectory of the particle that barely escapes capture (see Figure 3). The single fiber efficiency due to convective Brownian motion can be calculated from the equation of convective diffusion with appropriate boundary conditions.

FLOW FIELD AROUND A FIBER IN A FILTER

Because of flow interference among neighboring fibers, the flow around a fiber in a filter differs from that around an isolated fiber. Approximate analytical expressions have been derived for the flow field, which can be used to solve the equation of particle motion and the equation of convective diffusion. Alternatively, CFD codes can be employed to obtain numerical solutions of the flow field.

The flow field given by Kuwabara[10] for viscous flow in an array of randomly distributed parallel circular cylinders placed traverse to the flow has been employed to evaluate the single fiber efficiency. Kuwabara solved the equation for two-dimensional steady flow for an annular area around a cylinder with two assumptions: (1) the vorticity and the normal velocity component vanished on the imaginary outer boundary and (2) the ratio of the cross-sectional area of the cylinder to the area defined by the outer boundary was equal to the volume fraction of solid cylinders in the entire three-dimensional space under consideration (the ratio is identical to the packing density when the flow field is applied to a filter). According to the solution, the effect of flow interference can be characterized in terms of the Kuwabara hydrodynamic factor

$$Ku = -\frac{\ln\alpha}{2} - \frac{3}{4} + \alpha - \frac{\alpha^2}{4} \quad (4)$$

The flow model is known as a cell model, because the flow field in a cell defined by the imaginary outer boundary is used to represent the flow around a fiber in a filter. The Kuwabara flow field is based on the assumption that the velocity of the gas vanishes on the cylinder surface. The assumption is not met if the fiber diameter is comparable with the mean free path of the gas molecules or the pressure is low. The nature of the flow around a fiber depends on the Knudsen number of the fiber: $Kn_f = 2\lambda/d_f$, where λ is the mean free path of the gas molecules (the mean free path is about 0.0645 μm for air molecules at 293 K and normal atmospheric pressure). The Kuwabara flow field is valid when Kn_f approaches zero (the continuum flow regime). For the slip flow regime (when Kn_f is relatively small but not approaching zero), Pich[11] gave an expression based on the Kuwabara model. A similar expression was derived by Yeh[12] using a different set of boundary conditions. These two expressions are given in the Appendix.

CAPTURE BY INERTIAL IMPACTION

Inertial impaction of a particle is related to the flow field around the particle, which is characterized in terms of the particle Reynolds number Re_p (= d_pU_p/ν, where d_p is the particle diameter, U_p is the particle velocity relative to the gas flow, and ν is the kinematic viscosity of the gas). For $Re_p < 1$, the governing parameter for inertial impaction is the Stokes number

$$Stk = \frac{\rho_p d_p^2 C U_p}{9\mu\, d_f} = \frac{2BmU_p}{d_f} \quad (5)$$

dx.doi.org/10.1021/ie300574m | Ind. Eng. Chem. Res. XXXX, XXX, XXX–XXX

where ρ_p is the particle density, C is the slip correction factor, μ is the viscosity of the gas, B is the mechanical mobility of the particle, and m is the particle mass. It follows from eq 5 that the Stokes number is proportional to the particle momentum and inversely proportional to the fiber diameter.

The slip correction factor, a correction to the Stokes friction coefficient for particles having a size comparable with or smaller than the mean free path of the gas molecules, can be evaluated from the following empirical equation:

$$C = 1 + \frac{\lambda}{d_p}\left[2.33 + 0.966\exp\left(-0.4985\frac{d_p}{\lambda}\right)\right] \quad (6)$$

The constants in the equation were determined from experiments using polystyrene latex particles 19.90, 100.7, and 269 nm in diameter for the particle Knudsen number ($Kn_p = 2\lambda/d_p$) between 0.5 and 83.[13]

The mechanical mobility of a particle is the inverse of the friction coefficient. For a spherical particle, it is given by

$$B = \frac{C}{3\pi\mu\, d_p} \quad (7)$$

For small Stokes number, the following equation can be used to calculate the single fiber efficiency due to inertial impaction:[14]

$$\eta_I = \frac{Stk}{2Ku^2}[(29.6 - 28\alpha^{0.62})R^2 - 27.5R^{2.8}] \quad (8)$$

where R ($= d_p/d_f$) is the interception parameter. The equation is valid for $0.01 < R < 0.4$ and $0.0035 < \alpha < 0.111$. It does not take into account the effect of aerodynamic slip at the gas−fiber interface.

CAPTURE BY INTERCEPTION AND CONVECTIVE BROWNIAN DIFFUSION

For $R < 0.2$ and $\alpha < 0.5$, the single fiber efficiency due to interception can be calculated from the following expression:[15]

$$\eta_R = \left(\frac{1-\alpha}{Ku}\right)\frac{R^2}{1+R} \quad (9)$$

It follows from eq 9 that a finer fiber is more efficient than a coarser fiber in intercepting particles. Derived with the Kuwabara flow field, eq 9 applies only to interception from continuum flow around a fiber.

The governing parameter for convective Brownian diffusion is the Peclet number

$$Pe = \frac{d_f U}{D} \quad (10)$$

where D is the particle diffusion coefficient and U is the flow velocity. The Peclet number is a measure of the relative importance of convection and diffusion. At a given temperature T, the coefficient of Brownian diffusion can be evaluated from the Stokes−Einstein expression

$$D = kTB \quad (11)$$

where k is Boltzmann's constant.

It follows from eqs 7 and 11 that the diffusion coefficient is proportional to the ratio C/d_p, in which the slip correction factor C also depends on the particle diameter. For nonspherical particles, such as nanoparticle aggregates, the diffusion-equivalent diameter should be used in eq 11. The size of nanoparticle aggregates is usually determined with a differential mobility analyzer (DMA) or a diffusion battery. In a diffusion battery, a nanoparticle chain aggregate tends to move in random orientation, and the diameter thus determined is the diffusion-equivalent diameter. On the other hand, the orientation of a nanoparticle chain aggregate of conductive material tends to be parallel to its motion relative to the gas flow in a DMA.[16] The electrical mobility diameter of a conductive chain aggregate determined with a DMA therefore differs from the diffusion-equivalent diameter. Experimental evidence indicates that aerosol particles of most materials behave like conductors in an electric field because they generally contain conductive contaminants.[17] For nanoparticle chain aggregates of low fractal dimension, Wang and Friedlander[18] proposed a method for calculating the diffusion-equivalent diameter from the electrical mobility diameter.

Submicron particles have relatively low diffusion coefficients and hence large Peclet numbers. The following equation can be used to determine the single fiber efficiency due to convective Brownian diffusion for such particles:[15]

$$\eta_D = 2.6\left(\frac{1-\alpha}{Ku}\right)^{1/3} Pe^{-2/3} \quad (12)$$

Eq 12 is based on the Kuwabara flow field and therefore does not account for the effect of aerodynamic slip at the gas−fiber interface. For real filters in which fibers are neither all perpendicular to the flow direction nor uniformly distributed, Lee and Liu made a correlation between $\eta PeR/(1+R)^{1/2}$ and $[(1-\alpha)Pe/Ku]^{1/3}R/(1+R)^{1/2}$ for experimental data and obtained an empirical equation for single fiber efficiency due to the simultaneous action of convective diffusion and interception. The experimental data covered the following ranges of parameter values: $0.0086 < \alpha < 0.151$, $0.05 < d_p < 1.3$ μm, $0.0045 < R < 0.12$, and $Stk < 0.22$. The empirical equation is identical to the sum of eqs 9 and 12, except that the numerical coefficients 1 and 2.6 are replaced by 0.6 and 1.6, respectively.

For nanoparticles, which have higher diffusion coefficients and hence smaller Peclet numbers, Wang et al.[19] gave the following empirical equation:

$$\eta_D = 0.84Pe^{-0.43} \quad (13)$$

The equation indicates lower dependence of single fiber efficiency on Pe than does eq 12. Wang et al. showed that the equation agreed reasonably well with the penetration data reported by Japuntich et al.[20] and Kim et al.[21] The data were obtained using three face velocities, 0.053, 0.1, and 0.15 ms^{-1}, and four standard filter media, which had effective fiber diameters of 1.9, 2.9, 3.3, and 4.9 μm respectively, and a packing density between 0.039 and 0.05. Subsequently, Yamada et al. used a glass fiber filter and a polypropylene fiber filter to study the effect of filter structure.[22] They found that the lower dependence on Peclet number could be explained if the nonuniformity in filter structure was taken into consideration.

For the single fiber efficiency due to the simultaneous action of convective diffusion and interception, Stechkina and Fuchs[23] used the Kuwabara flow field to derive the following equation:

$$\eta_{DR} = 2.9Ku^{-1/3}Pe^{-2/3} + 0.624Pe^{-1} + \eta_R + \frac{1.24R^{2/3}}{(KuPe)^{1/2}} \quad (14)$$

dx.doi.org/10.1021/ie300574m | Ind. Eng. Chem. Res. XXXX, XXX, XXX−XXX

The single fiber efficiency due to interception, η_R, can be calculated from eq 9. Eq 14 is valid for $R < 0.5$ and $Ku/Pe < 0.024$.

For single fiber efficiency due to convective diffusion and interception from slip flow around a fiber, Payet[24] (see also Payet et al.[25]) suggested the following equation:

$$\eta_{DR} = \frac{1.6Ka^{1/3}Pe^{-2/3}(1 + 0.388Ka^{1/3}Pe^{1/3}Kn_f)}{1 + 1.6Ka^{1/3}Pe^{-2/3} + 0.621Ka^{2/3}Pe^{-1/3}Kn_f} + 0.6Ka\frac{R^2}{1+R}\left(1 + \frac{1.999Kn_f}{R}\right) \quad (15)$$

where $Ka = (1 - \alpha)/Ku$. Eq 15 is a generalization of eqs 9 and 12 to account for the effect of aerodynamic slip at the gas−fiber interface. Payet et al. showed that calculations from the equation were in good agreement with the data obtained from filtration experiments using particles 0.08 to 0.4 μm in diameter, Teflon-coated glass fiber filters (thickness = 0.24 mm, packing density = 0.08, mean fiber diameter = 1 μm), and a face velocity of 0.0365 ms^{-1}.[25]

CAPTURE BY COULOMBIC AND DIELECTROPHORETIC FORCES

Although most aerosol particles and fibers in a filter carry some electric charges, the charge levels are not sufficiently high for electrostatic deposition to become significant. A simple approach to take advantage of electrostatic forces is to employ highly charged fibers, such as in an electret filter. Coulombic and dielectrophoretic forces play a central role for particle collection by an electret filter composed of bipolar charged fibers. For a charged particle moving in an electret filter, the governing parameter for deposition due to Coulombic force is

$$K_C = \frac{Cn_p e\bar{\sigma}}{6\varepsilon_0(1 + \varepsilon_f)\mu d_p U} \quad (16)$$

where n_p is the number of electronic charges on the particle, e is the charge of an electron, $\bar{\sigma}$ is the average charge density on the fiber (= $2/\pi$ times the maximum charge density for a sinusoidal distribution of surface charges), ε_0 is the vacuum permittivity, and ε_f is the dielectric constant of fiber. The dimensionless parameter K_C is proportional to the drift velocity of the particle due to Coulombic force and inversely proportional to the flow velocity.

The governing parameter for deposition due to the dielectrophoretic force acting on a neutral particle in an aerosol flow is

$$K_{In} = \frac{(\varepsilon_p - 1)C\pi^2\bar{\sigma}^2 d_p^2}{6\varepsilon_0(\varepsilon_p + 2)(\varepsilon_f + 1)^2\mu d_f U} \quad (17)$$

where ε_p is the dielectric constant of the particle. Similar to K_C, the dimensionless parameter K_{In} is proportional to the drift velocity due to dielectrophoretic force and inversely proportional to the flow velocity.

Using the expression for electrostatic field around an isolated fiber, Brown[26] analyzed capture of charged and neutral particles by electrostatic forces and interception in an electret filter composed of bipolar charged fibers with a random orientation of line dipoles. His results for various types of flow field, including the Kuwabara model, indicate that there exists a critical value of interception parameter, R_C, below which the interception mechanism plays no role in particle collection. Brown's paper shows that the value of R_C varies with the orientation of line dipole, but the equation given for single fiber efficiency due to Coulombic forces does not include the effect of interception. Subsequently, Pich et al.[27] derived the following expression for single fiber efficiency due to Coulombic forces and interception for the same type of electret filter:

$$\bar{\eta}_{CR} = \eta_R + K_C\left[\frac{1}{1+R} - \frac{\eta_R}{(1+R)\eta_R + K_C}\right] \quad (18)$$

Although the expression includes the effect of interception, it does not take into consideration the existence of a critical value of interception parameter.

Otani et al.[28] compared the results of the two studies cited above and proposed the following expressions for single fiber efficiency due to Coulombic forces and interception for an electret filter with randomly distributed orientations of line dipole:

For $R < R_C$ and $10^{-3} < K_C < 10^{-1}$,

$$\bar{\eta}_{CR} = 0.78K_C \quad (19)$$

For $R < R_C$ and $10^{-1} < K_C < 10$,

$$\bar{\eta}_{CR} = 0.59Ku^{-0.17}K_C^{0.83} \quad (20)$$

where $R_C = 0.66\ (K_C Ku)^{0.64}$. For $R > R_C$, eq 18 should be used.

To calculate the single fiber efficiency due to dielectrophoretic force for an electret filter with randomly distributed orientations of line dipole, Otani et al. suggested the following equations:

For $R = 0$ and $10^{-4} < K_{In} < 10^{-2}$,

$$\eta_{In} = 1.48K_{In}^{-0.93} \quad (21)$$

For $R = 0$ and $10^{-2} < K_{In} < 10^{0}$,

$$\eta_{In} = 0.51Ku^{-0.35}K_{In}^{0.73} \quad (22)$$

For $R = 0$ and $10^{0} < K_{In} < 10^{2}$,

$$\eta_{In} = 0.54Ku^{-0.6}K_{In}^{0.4} \quad (23)$$

PRESSURE DROP

The pressure drop across a filter arises mainly because of the resistance of individual fibers to flow. In a filter with a low packing density, the gas flow follows Darcy's law and the pressure drop can be expressed in terms of the packing density α, the face velocity U_0, and the filter thickness L:

$$\Delta p = \frac{\mu L U_0 f(\alpha)}{d_f^2} \quad (24)$$

By making a correlation between α and $\Delta p d_f^2/\mu L U_0$ for a large number of experimental data, which covered the range of fiber diameter from 1.6 to 80 μm and the range of α from 0.006 to 0.3, Davies[29] obtained the following expression:

$$f(\alpha) = 64\alpha^{1.5}(1 + 56\alpha^3) \quad (25)$$

According to Davies,[5] the scatter of data about eq 24 was mostly less than ± 30%. Werner and Clarenburg[30] further tested the equation using glass fiber filters. Their data for $0.039 < \alpha < 0.084$ and geometric mean diameter of fibers between 0.097 and 1.53 μm were in good agreement with the correlation equation.

dx.doi.org/10.1021/ie300574m | Ind. Eng. Chem. Res. XXXX, XXX, XXX−XXX

Table 1. Experimental Studies on Thermal Rebound Using Wire Screens, Tubes, and Fibrous Filters

investigators	particle collectors	flow rate, face velocity	particles	classifying and counting instruments	results
wire screens					
Otani et al.[38]	stainless steel, d_s: 4.2 cm, d_f: 52, 300 μm, α: 0.293, 0.31	U_0: 0.012−0.036 ms^{-1}	silver	DMA, electrometer	rebound observed for particles <1 nm, size questionable
Ichitsubo et al.[39]	stainless steel, d_s: 3.2 cm, d_f: 75 μm, α: 0.289	Q: 6 L/min	silver, NaCl, C_6H_6-H_2O, ion clusters	DMA, electrometer	rebound observed for particles and ion clusters <2 nm, size questionable
Alonso et al.[40]	stainless steel, d_s: 1.1, 3.2 cm, d_f: 75 μm, α: 0.289	Q: 1, 3, 6 L/min	silver, NaCl, charged and uncharged	a tandem DMA system, CNC	no rebound effect for particles down to 2 nm and for 1.36-nm ions
Heim et al.[41]	grounded nickel, d_s: 2.2 cm, d_f: 54.6 ± 0.9 μm, α: 0.34	Q: 1.5 L/min	NaCl, charged and uncharged	DMA, CPC	no rebound effect for particles down to 2.5 nm
Shin et al.[44]	stainless steel, d_s: 4.7 cm d_f: 90 μm, α: 0.3105	U_0: 0.0417−0.095 ms^{-1}	silver	nano-DMA, ultrafine CPC	no rebound effect for particles down to 3 nm at 500 K
Heim et al.[45]	nickel and stainless steel, d_s: 5.3 cm, d_f: 50.1−101.2 μm, α: 0.297−0.335	U_0: 0.113−0.165 ms^{-1}	singly charged WO_x, THAB ions	high flow DMA, electrometer	no rebound effect for particles down to 1.2 nm
Mouret et al.[37]	stainless steel, d_f: 25 μm	U_0: 0.05 ms^{-1}	copper	nano-DMA, CPC	no rebound effect for particles down to 4 nm
tubes					
Otani et al.[38]	aluminum, d_t: 0.6 cm	Q: 1−3 L/min	silver	DMA, electrometer	rebound observed for particles <2 nm, size questionable
Alonso et al.[40]	stainless steel, d_t: 0.4 cm	Q: 1, 3, 6 L/min	silver, NaCl, charged and uncharged	a tandem DMA system, CNC	no rebound effect for particles down to 2 nm and for 1.36-nm ions
fibrous filters					
Kim et al.[42]	glass fibers, d_F: 4.15 cm, d_f: 9.1, 11.8 μm	U_0: 0.025 ms^{-1}	NaCl, charged and uncharged	nano-DMA, particle size magnifier-CNC	rebound observed for particles <2 nm
Huang et al.[43]	respirators, d_F: 10.8 cm, d_f: 13 μm, α: 0.035	Q: 30, 60, 85 L/min	NaCl	long-DMA, nano-DMA, CPC	no rebound effect for particles down to 4.5 nm
Kim et al.[21]	glass fibers, electret, e-PTFE membrane, A_F: 17.34 cm^2, d_f: 1.9−4.9 μm, α: 0.039−0.05	U_0: 5.3, 10, 0.15 ms^{-1}	silver	nano-DMA, ultrafine CPC	no rebound effect for particles down to 3 nm

It follows from eq 24 that pressure drop is proportional to the filter thickness and inversely proportional to the square of the fiber diameter. Pressure drop is also proportional to the face velocity, because the flow in a filter is laminar. Data on pressure drop have been used with eq 24 to determine an effective fiber diameter, which can be applied to calculations of collection efficiency from eq 3.

The pressure drop across a filter can be calculated as the sum of the drag on all fibers. By generalizing the Kuwabara flow field to account for aerodynamic slip at the gas−fiber interface, Pich obtained the following expression:[31]

$$\Delta p = \frac{16\mu L U_0 \alpha (1 + 1.996 Kn_f)}{d_f^2 \left[Ku + 1.996 Kn_f \left(-\frac{1}{2}\ln \alpha - \frac{1}{4} + \frac{\alpha^2}{4} \right) \right]} \quad (26)$$

Eq 26 is identical to eq 24, except that the function $f(\alpha)$ in eq 24 is replaced by a function of α and Kn_f in eq 26. The equation predicts a pressure drop higher than experimental measurements using real filters.

THERMAL REBOUND

Under normal conditions, the gas molecules that do not adsorb on surfaces can pass through a fibrous filter freely. Will a nanoparticle escape capture by a filter as well, if it is sufficiently small? A particle striking a solid surface will rebound if the kinetic energy of the particle exceeds the adhesion energy and there is no energy loss during impact. The threshold impact velocity above which rebound takes place is called the critical velocity. The velocity at which a particle strikes a surface is approximately equal to its thermal velocity. If the thermal velocity of aerosol particles is assumed to follow the Maxwell−Boltzmann distribution, the mean thermal velocity is inversely proportional to the particle diameter raised to a power of 1.5. It follows that the mean thermal velocity will exceed the critical velocity for a sufficiently small particle.

An energy balance for the particle−surface impact gives the following expression for the critical velocity:

$$V_{cr} = \left(\frac{2E_{ad}}{m} \right)^{1/2} \quad (27)$$

where E_{ad} is the adhesion energy and m is the particle mass. Eq 27 assumes that there is no energy loss during impact. The assumption is reasonable for nanoparticles because the contact duration is probably too short for a complete plastic deformation.[32]

As data on material properties are lacking, it is difficult to derive an expression for the adhesion energy from the dynamic impact equation of particle motion. A common practice is to use the adhesion theories developed from static equilibrium conditions, such as the models proposed by Bradley,[33] Hamaker,[34] and Johnson et al.[35] In their analysis for thermal rebound, Wang and Kasper[32] found that the JKR (Johnson, Kendall, and Roberts) model and the B-H (Bradley−Hamaker) model gave similar values of critical velocity. They decided to use the JKR model, because the B-H model assumed a point contact, whereas in reality adhesion force could develop a finite contact area between the particle and the surface. With the JKR model, Wang and Kasper obtained the following expression for the critical velocity:

$$V_{cr} = \left[\frac{3^7 \pi^4 (K_p + K_s)^2 \sigma_{p,s}^5}{\rho_p^3 d_p^5} \right]^{1/6} \quad (28)$$

In the above equation, $\sigma_{p,s}$ is the specific adhesion energy at interfacial contact area. K_p and K_s are, respectively, the

dx.doi.org/10.1021/ie300574m | Ind. Eng. Chem. Res. XXXX, XXX, XXX−XXX

mechanical constants for the particle and the surface material, which can be calculated from the Poisson ratio and Young's modulus.

It follows from eq 28 that the critical velocity is proportional to the specific adhesion energy raised to a power of 5/6 and inversely proportional to the particle diameter raised to the same power. For the following values of parameters: T = 273 K, $(K_p + K_s) = 5 \times 10^{-11}$ m^2 N^{-1}, and ρ_p = 1000 kg m^{-3}, the critical velocity calculated from eq 28 is equal to the mean thermal velocity of a 0.6-nm particle if $\sigma_{p,s}$ = 0.04 J m^{-2} and equal to the mean thermal velocity of an 8-nm particle if $\sigma_{p,s}$ = 0.005 J m^{-2}. From these results, Wang and Kasper suggested that the mean thermal impact velocity would exceed the critical velocity in the particle size range between 1 and 10 nm. It was difficult to predict a narrower range for the onset of thermal rebound, because values of the physical parameters required in calculations had not been accurately determined.

According to a paper published by Johnson in 1997,[36] the B-H model provides a good approximation when elastic deformation is negligible and the JKR model is good when the magnitude of the elastic deformation cannot be neglected. Recently, Mouret et al.[37] calculated the Tabor parameter relating the magnitude of the elastic deformation and the range of surface forces, and from the calculations they concluded that the B-H model was more appropriate for evaluating the adhesion energy of the nanoparticle−fiber system. Using a more exact formula of the B-H model and 6.4×10^{-20} J for the Hamaker constant, they found that the decrease in adhesion efficiency due to thermal rebound began for particles about 3 nm in diameter. Based on the calculations with a range of values for the Hamaker constant, they suggested that the downward trend in capture efficiency due to thermal rebound might occur only for particles smaller than 1 nm. The adhesion efficiency declines gradually with decreasing particle size, because the thermal velocity of particles follows the Maxwell−Boltzmann distribution. As a result, the downward trend of capture efficiency, which increases with decreasing particle size in the absence of thermal rebound, begins at a particle size smaller than the onset of the decline in adhesion efficiency. According to the calculations of Mouret et al., the effect of thermal rebound increases with increasing temperature, but it is necessary to raise the temperature to about 1000 K before the effect becomes observable.

Experimental studies on collection of nanoparticles in fibrous filters, wire screens, and laminar flow tubes have provided data on penetration or collection efficiency as a function of particle size.[21,37−45] In all the studies listed in Table 1, no effect of thermal rebound is observed for particles as small as 2 nm. Some experiments indicate that the effect is observable for particles smaller than 2 nm, but questions have been raised regarding the accuracy of particle size determination.[39−41]

Molecular dynamics simulations for collisions of nanoparticles with a surface have not yielded results showing the effect of thermal rebound. Sato et al.[46] performed simulations for collision dynamics of silver, nickel, and silica particles, 0.5−2 nm in diameter, with a silver surface. They found that, at room temperature, only a tiny fraction of nanoparticles in the upper end of the Maxwellian energy distribution had sufficiently high energy to bounce off the surface. Subsequently, Jung et al.[47] investigated collisions of a Lennard−Jones particle comprising 1055 molecules (equivalent to a 2.7-nm copper particle) onto a weakly attractive rigid surface using the molecular dynamics simulation. Their results suggested that no thermal rebound effect was expected for the particle studied.

EFFECTS OF PARTICLE SHAPE AND AGGREGATE MORPHOLOGY

Particle shape has been shown to affect the collection efficiency for nanoparticles in fibrous filters. Boscovic et al.[48] carried out experiments with polystyrene latex (PSL) spheres, spherical particles of iron oxide, and perfect cubes of magnesium oxide. The polypropylene filter used in the experiments was 2 mm thick and had a packing density of 0.09. The fiber diameter and the face velocity were, respectively, 19 μm and 0.02 ms^{-1}. The results showed that, for particle sizes in the range of 50 to 300 nm, the collection efficiencies for cubic particles were much lower than for spherical particles of the same electrical mobility diameter and the difference in efficiency increased with increasing particle size. The explanation given by Boscovic et al. is that particles of different shapes move differently on the fiber surface immediately following collision: spherical particles slide or roll before coming to rest, whereas cubic particles slide or tumble. Tumbling can significantly change the contact area between a cubic particle and the fiber surface, thereby increasing the probability for the particles to detach from the fiber. It should be noted that detachment due to tumbling differs from thermal rebound discussed in the preceding section.

In a subsequent study,[49] a 3-mm thick polypropylene filter was soaked with mineral oil and then squeezed to remove excess oil. After this procedure, the filter had a packing density of 0.184 and the fiber had a mean diameter of 12.9 μm with a standard deviation of 1.4. Collection efficiencies of spherical PSL particles and cubic MgO particles, 50−300 nm in electrical mobility diameter, were determined for two face velocities, 0.1 and 0.2 ms^{-1}. No significant difference was observed in collection efficiency between spherical and cubic particles of the same electrical mobility diameter. The results indicated that absorption of the kinetic energy of particles by the oil film had effectively restrained particle motion on the fiber after collision and thereby reduced the probability for the particles to detach from the surface. The finding supports the explanation that the type of particle motion on the fiber surface after collision can influence collection efficiency.

To further examine the effects of particle shape and particle velocity on the collection efficiency for nanoparticles, Boscovic et al.[50] conducted experiments with spherical PSL particles, perfect cubes of MgO particles, and cubic NaCl particles with rounded corners. The 2-mm thick polypropylene filter used in the experiments had a packing density of 0.29 and a fiber diameter of 12 μm. The experiments were carried out with three face velocities, 0.05, 0.1, and 0.2 ms^{-1}. The results showed that, when inertial effects were negligible at U_0 = 0.05 and 0.1 ms^{-1}, the collection efficiencies for 100-nm particles were in the following order: PSL particles > NaCl particles > MgO particles. The order can be explained in terms of the type of particle motion on the fiber surface as follows: a cubic NaCl particle with rounded corners will tumble if it hits a fiber with one of its sharp edges, but will roll if it hits a fiber with one of its rounded corners. As a result, the intermediate shaped NaCl particles have a detachment probability between those of spheres and perfect cubes. At U_0 = 0.2 ms^{-1}, there is no significant difference in collection efficiency between cubic MgO particles and intermediate shaped NaCl particles, because the increase in collection efficiency due to inertial impaction for

dx.doi.org/10.1021/ie300574m | Ind. Eng. Chem. Res. XXXX, XXX, XXX−XXX

the denser (and hence heavier) MgO particles sufficiently offsets the higher detachment probability.

Nanoparticle agglomerates are generally in the shape of chains or clusters. Effect of agglomerate morphology on collection efficiency has been studied. Kim et al. performed filtration experiments using silver nanoparticle agglomerates with electrical mobility diameter between 50 and 300 nm.[51] The agglomerates consisted of primary particles with a mean diameter of 16.2 nm and an estimated standard deviation of 3.1 nm. To generate agglomerates of various structures, the agglomerates were sintered in a tube furnace at temperatures in the range between room temperature and 873 K. The maximum projected length of sintered agglomerates differed according to the sintering temperature. For example, the means of the maximum projected length of 100-nm (electrical mobility diameter) agglomerates were 203.13 and 156.17 nm for agglomerates sintered at room temperature and 473 K, respectively, and the sintered agglomerates were nearly spherical at a sintering temperature of 873 K. The filtration experiments were carried out at a face velocity of 0.053 ms^{-1} using a 0.53-mm thick fiberglass filter, which had an effective fiber diameter of 1.9 μm and a packing density of 0.05. The results indicated that, for agglomerates of the same electrical mobility diameter, the penetration decreased with increasing projected length of the agglomerate. Model calculations showed that interception was an important contributor to capture of these agglomerates and the interception parameter calculated using the maximum projected length, instead of the electrical mobility diameter, was able to explain reasonably well the difference in collection efficiency between agglomerates of different structures.

It has also been found that multiwalled carbon nanotubes (MWCNTs) are removed by fibrous filters at a higher efficiency than are spherical particles of the same mobility diameter.[52] The MWCNT particles used in the experiments had an electrical mobility diameter of 300 nm. They were fibrous in shape, about 60 nm in diameter, and 2.1 μm long. The aerosol stream passed through a 0.38-mm thick glass fiber filter with a packing density of 0.049 and an average fiber diameter of 2.8 μm, at face velocities ranging from 0.05 to 0.5 ms^{-1}. Single fiber efficiencies calculated from the penetration data indicated that interception was the dominant capture mechanism and the preferred orientation of the fibrous particles around the fiber played an important role.

MODERATE FIBER REYNOLDS NUMBERS

The Kuwabara flow field is valid only for small fiber Reynolds number ($Re_f = d_f U/\nu$). In the transition (from viscous to inertial) flow regime, for which Re_f is in the range of 1 to 15, the inertial force becomes appreciable and in consequence the streamlines approaching a fiber turn around more sharply. Some industrial filters are operated at such moderate fiber Reynolds numbers. Hubbard et al.[53] conducted a study on collection efficiency and pressure drop in the transition flow regime, using cotton fiber filters with a packing density of 0.1 and a fiber diameter of 15 μm. Cubic NaCl particles and iron nanoparticle agglomerates with geometric mean diameters of 85 and 97 nm, and geometric standard deviations of 2.0 and 1.5, respectively, were used in the tests. These two types of particles were selected because of dissimilar densities and shape factors. The filtration experiments were carried out with two pressures (20.2 and 80.8 kPa), three temperatures (253, 273, and 293 K), and face velocities between 5 and 19 ms^{-1}. Under these conditions, the fiber Reynolds number was in the range between 1 and 15. As expected, the pressure drop data did not follow the linear relationship with face velocity given in eq 24. Instead, the dimensionless pressure drop ($= \Delta p/\rho_g U_0^2$, ρ_g being the gas density) agreed well with a nonlinear expression derived by Robinson and Franklin.[54] For both types of test particles, the filtration efficiencies for the same fiber Reynolds number correlated well with the Stokes number, indicating the important roles played by inertial impaction and transition flow under the test conditions. At the same face velocity, collection efficiency increased with decreasing pressure as a result of reduction in the frictional resistance to the gas flow. Hubbard et al. also pointed out that, in the transition flow regime, the flow field was likely to vary along the depth of a fibrous filter, which would lead to nonuniformity of single fiber efficiency.

Inertial fibrous filters have been developed as an alternative to low pressure impactors for sampling and classifying nanoparticles for chemical analysis.[55] The 8-mm thick filter used in the tests was made of stainless steel fibers, 8 μm in diameter. The packing density of the filter was 0.0065 and the face velocity was in the range 0.05−50 ms^{-1}. At 50-ms^{-1} face velocity, the pressure drop across the filter was 28 kPa, compared with 90 kPa across a low pressure impactor. The filter was able to maintain its structure at high filtration velocities because of its compressive strength. Polydisperse $ZnCl_2$ particles, between 6 and 200 nm in diameter, were used as test particles. The results showed that inertial impaction was the dominant capture mechanism at higher velocities and, at a face velocity of 50 ms^{-1}, a 50% cutoff was achieved for particles as small as 50 nm in diameter. The 50% cutoff size, which decreases with increasing filtration velocity, can be predicted from $Stk = 1$ (the value of the Stokes number that gives 50% collection efficiency). Because the inertial fibrous filter can be operated at high flow rates, it can be employed as a portable device for rapid collection of nanoparticle samples. Furthermore, the pressure drop across an inertial fibrous filter is significantly lower than across a low pressure impactor and therefore can minimize evaporation losses of semivolatile components in the captured particles.

In a subsequent study,[56] an inertial fibrous filter was combined with a four-stage impactor to form a complete system, named Nanosampler, for sampling and classifying ambient aerosols in six size fractions for chemical analysis. The 5.5-mm thick filter, made of stainless steel fibers 9.8 μm in diameter, had a packing density of 0.0135 and a diameter of 4.75 mm. At a flow rate of 40 L/min, the cutoff size was about 65 nm. Results of field tests indicated that the inertial fibrous filter performed satisfactorily.[57]

EFFECT OF HUMIDITY

Kim et al. found that the collection efficiency for monosized NaCl particles, 3−70 nm in diameter, was independent of humidity.[42] The experiments were conducted using a 0.4-mm-thick filter made of glass fibers with a mean diameter of 9.1 μm. A neutralizer (^{241}Am) was employed to reduce the charges on test particles to the Boltzmann equilibrium distribution. For three relative humidity levels (0.04%, 1.22%, and >92%) and a face velocity of 0.025 ms^{-1}, the results showed that the filtration efficiency differed only slightly at different humidity levels. This is in contrast to larger particles, for which the collection efficiency increases with increasing humidity.[58]

dx.doi.org/10.1021/ie300574m | Ind. Eng. Chem. Res. XXXX, XXX, XXX−XXX

EFFECTS OF FIBER DIAMETER

From eqs 14 and 15, it can be seen that the single fiber efficiency due to interception acting together with convective Brownian diffusion is higher for finer fibers. In addition, eq 3 indicates that filtration efficiency increases with decreasing fiber diameter and increasing single fiber efficiency. One would therefore expect that filters composed of finer fibers offer a better choice for nanoparticle collection. However, it follows from eqs 24 and 26 that decrease in fiber diameter leads to increase in pressure drop as well. A commonly used index of filter performance is the quality factor, also known as figure of merit, which is defined as the ratio $\ln(1/P)/\Delta p$. Hinds[8] calculated the collection efficiency as a function of particle size for three filters having the same pressure drop, packing density (0.05), and face velocity (0.1 ms^{-1}). The three filters were composed of fibers 0.5, 2, and 10 μm in diameter respectively. The results showed that the most penetrating particle size (MPPS) was smaller and the minimum efficiency was higher for the filter composed of finer fibers. However, the filter with finer fibers gave a higher quality factor only for particles larger than 0.2 μm in diameter.

The term nanofiber has been used to denote fibers smaller than 1 μm in diameter (some set the upper limit as 0.5 μm). Filtration experiments with nanofiber filters have largely confirmed Hinds' calculations cited above. Podgórski et al. carried out experiments using five dual-layer filters composed of a polydisperse nanofiber mat and a polydisperse microfiber mat for collection of polydisperse liquid DEHS particles, 10−500 nm in diameter, at a face velocity of 0.0894 ms^{-1}.[59] The nanofibers, produced by a modified melt-blown method, had mean diameters between 0.74 and 1.41 μm. The five nanofiber mats had thicknesses ranging from 1.4 to 5.5 mm, and packing densities from 0.014 to 0.035. The mean diameter of microfibers was 18 μm, and the microfiber mat had a thickness of 2.1 mm and a packing density of 0.149. The results showed that the collection efficiency of all five dual-layer filters for particles in the MPPS range was significantly higher than the efficiency of the microfiber mat tested alone. Because the increase in pressure drop due to addition of one nanofiber mat was quite moderate, four of the five dual-layer filters had quality factors higher than that of the microfiber mat. Only one dual-layer filter tested had a lower quality factor for particles smaller than 30 nm in diameter. Based on these findings, Podgórski et al. recommended a triple-layer design for filtration of polydisperse aerosols containing nanoparticles: a thin microfiber mat composed of densely packed coarse fibers used as a support, a thicker and more porous mat of nanofibers used as a middle layer, and a thick and porous mat composed of fibers a few micrometers in diameter used as a front layer to collect micrometer particles and hence shield the middle layer from coarse particles.

Yun et al.[60] used polyacrylonitrile nanofiber filters to study collection of monodisperse NaCl particles 10 to 80 nm in diameter at the face velocity of 0.053 ms^{-1}. The nanofibers, 0.27 μm in diameter, were produced using the electrostatic spinning process. The five nanofiber filters used in the tests had thicknesses ranging from 0.004 to 0.02 mm and packing densities from 0.112 to 0.152. For comparison, one nanofiber filter composed of 0.4-μm polyacrylonitrile fibers, two commercial medium-grade polyolefin fiber filters, a high-efficiency particulate air (HEPA) filter, and an ultra-low-penetration air (ULPA) filter were also tested under the same conditions. The results showed that, to achieve the same level in collection efficiency as commercial filters, the nanofiber filters required a substantially lower mass but a higher pressure drop. For a given particle size, the filter quality factor and single fiber efficiency for nanofiber filters depended primarily on packing density and fiber diameter.

Wang et al. conducted a study using four test filters, each composed of a layer of nanofibers placed on a substrate made of micrometer fibers.[61] The nanofibers were 0.15 μm in diameter, the effective packing density in the range 0.034−0.134, the face velocity 0.10 ms^{-1}, and the particle diameter in the range 3−780 nm. They found that both filtration efficiency and pressure drop increased with increase in packing density of the nanofiber layer. Because of significant increase in pressure drop, the addition of nanofibers was able to improve the filter quality factor only for particles larger than about 100 nm in diameter. Wang et al. also developed a numerical model for nanofiber filters. The simulation results agreed well with experimental data for particles larger than 20 nm.

Leung et al. carried out experiments with nanofibers coated on a microfiber substrate to determine the effects of face velocity, filter thickness, and packing density on filtration efficiency and pressure drop.[62] The substrate, composed of fibers with a mean diameter of 14.7 μm, had a packing density of 0.13 and negligible filtration efficiency and pressure drop. The polyethylene oxide nanofibers, produced by the electrostatic spinning process, had a mean diameter of 208 nm and the test particles were 50 to 480 nm in diameter. Four nanofiber filters, with thicknesses between 11.4 and 17.2 μm and packing densities between 0.0039 and 0.036, were tested at two face velocities, 0.05 and 0.1 ms^{-1}. The results showed that the most penetrating particle size decreased with increase in packing density and the filtration efficiency generally decreased with increase in face velocity. The filter thickness appeared to have less prominent effect on MPPS than did the packing density. Leung et al. therefore suggested stacking up multiple filters to improve performance.

In a subsequent study with three sizes of electrospun Nylon 6 nanofibers, 94, 185, and 220 nm in diameter, Hung and Leung showed that the filters of finer nanofibers gave higher filtration efficiencies for particles 50−200 nm in diameter than did filters of coarser nanofibers, mainly because of enhancement in convective diffusion and interception.[63] However, the pressure drop was significantly higher for the filters of finer nanofibers. For collection of 50−90 nm particles, the filter of 185-nm fibers had a quality factor higher than the filter of 94-nm fibers had, but the order of quality factor was reversed for collection of 100−380 nm particles. These experiments were conducted with the fiber Knudsen number in the range 0.617−1.443 and the Peclet number between 0.54 and 21.39.

It has been shown that growing multiwalled carbon nanotube (MWCNT) fibers on a fibrous filter can enhance the capture efficiency for nanoparticles without appreciable increase in pressure drop. By catalytically activating glass fiber surfaces with iron nanoparticles generated using a spark discharge method, Park et al. grew MWCNT fibers on the activated surfaces in a thermal chemical vapor deposition reactor.[64] The 0.5-mm thick filter was composed of glass fibers 3 μm in average diameter and had a packing density of 0.35. The MWCNT fibers grew in random directions on glass fibers and were smaller than 100 nm in diameter. The iron nanoparticles had a geometric mean diameter of 38.5 nm and the mass of iron nanoparticles deposited per cm^2 of the filter was estimated to be 33.5 μg.

dx.doi.org/10.1021/ie300574m | Ind. Eng. Chem. Res. XXXX, XXX, XXX−XXX

Potassium chloride particles, between 15 and 750 nm in diameter, and a face velocity of 0.5 ms^{-1} were used in the filtration experiments. The results showed that filtration efficiency increased from 8 to 15% for 100-nm particles (in the most penetrating particle size range) after MWCNT fibers were grown on the glass fibers. Furthermore, the MWCNT-deposited filter was found to be capable of inactivating 83.7% of *E. coli*, when the glass fiber filter was used as a control.

EFFECT OF PARTICLE LOADING ON THE PERFORMANCE OF NANOFIBER FILTERS

When solid particles just begin to deposit on a clean fiber, captured particles scatter over the fiber surface sparsely. Smaller in size than a fiber and protruding further into the aerosol stream, a deposited particle is more efficient than a fiber in capturing particles. A dendrite or irregular chain-like aggregate is formed when a deposited particle captures another particle. Further deposition leads to growth of dendrites, which eventually bridge together to form a dust cake. The formation and growth of particle dendrites can be explained with two intrinsic properties of aerosol particles: the particles are of finite size and are randomly distributed in an aerosol stream.[65] The shape and location of particle deposits on a fiber vary with the dominating capture mechanism.[66,67] For many types of filters, penetration decreases exponentially, whereas pressure drop increases exponentially, with specific deposit (mass of particles captured per unit area of filter). Growth of dendrites and effects of particle loading on filter performance have been extensively studied for decades, but are not yet well understood. Davies[5] and Brown[6] gave detailed reviews of the findings published before 1993. Later studies include Schmidt,[68] Endo et al.,[69] Thomas et al.,[70] Brown and Wake,[71] Sakano et al.,[72] Kanaoka et al.,[73] Ji et al.,[74] Tanthapanichakoon et al.,[75] Song et al.,[76] Saelim et al.,[77] Kim et al.,[78] and Kasper et al.[79]

At present there are only a few published studies of the performance of nanofiber filters under continuous loading conditions. Leung and Hung investigated the effects of particle loading on filtration efficiency and pressure drop for three nanofiber filters and one microfiber filter at a face velocity of 0.05 ms^{-1}.[80] The filters were made of fibers 0.3 and 1.8 μm in diameter respectively. The three nanofiber filters were 0.01 mm in thickness and had packing densities in the range 0.01078−0.02403. The nanofiber web in each filter was coated on a coarse fibrous structure, which had negligible filtration efficiency and pressure drop. The thickness and packing density of the microfiber filter were 0.1 mm and 0.04845, respectively. Monosized NaCl particles, 41−514 nm in electrical mobility diameter, were used as test particles. To study the effects of particle loading, polydisperse NaCl aerosols were employed to load the filters. They found that the filtration efficiencies of clean nano- and microfibrous filters for particles smaller than 70 nm were in good agreement with the calculations from eq 15. The most penetrating particle size (MPPS) was 103 and 203 nm, respectively, for nano- and microfibrous filters before they were loaded with particles. Particle loading led to decrease in MPPSs for both types of filters, and the decrease was larger for nanofiber filters than for microfiber filters. The increase in pressure drop across a nanofiber filter approximately followed a third degree polynomial function of specific deposit. Under continuous loading conditions, the rate of increase in pressure drop was lower for the microfiber filter than for nanofiber filters.

In a subsequent study, Leung et al. used the same experimental setup to test three types of dual-layer filters.[81] The results showed that, under continuous loading conditions, the dual-layer filter consisting of a microfiber layer in front of a nanofiber layer had a lower rate of increase in pressure drop than did the dual filter with a reverse stacking order. The dual-layer filter with the micro-nano stacking order was able to make use of the favorable features of nanofibers in the initial stage of filtration and those of microfibers in the loaded stage.

CONCLUDING REMARKS

A review of the classical theory of fibrous filters and recent developments in nanoparticle collection is presented. The review of the current status of this field covers thermal rebound and effects of particle shape, aggregate morphology, flow regime, humidity, fiber size, and particle loading. While recent years have seen many advances in these areas, many more studies are needed to improve our capabilities in filter design for nanoparticle collection.

Since Wang and Kasper[32] published their analysis of thermal rebound of nanoparticles, the problem has received considerable attention. Recent calculations of Mouret et al.[37] show that the effect of thermal rebound on collection efficiency probably can be observed only for particles smaller than 1 nm in diameter. More accurate experiments are required, but classifying and counting instruments for subnanoscale particles are not yet available. On the other hand, it is likely that molecular dynamics simulations for collisions of ion clusters with nanofibers could yield useful results for comparison with the calculations of Mouret et al.

Particle shape and aggregate morphology are distinct physical properties of nanoscale particles, which have been shown to have marked effect on collection efficiency. More effort is needed to gain a better understanding of their role in deposition and adhesion on a fiber, especially on a nanofiber. The effect of humidity on collection efficiency for nanoparticles also deserves further experiments and theoretical analyses. The results should have practical applications in designing filters for humid environments, such as disposable respirators, industrial gas cleaning equipment, automotive cabin air filters, and indoor air purifiers.

Theoretical analyses of single fiber efficiency have been mostly based on approximate analytical expressions for flow field. In recent years, the lattice-Boltzmann model[82] and the Fluent computational fluid dynamics code[83,84] have been employed to calculate the flow field in a fibrous filter. These approaches entail a considerable amount of computations, but have versatility in dealing with nonuniform filter structures. Further developments of these approaches are likely to facilitate their application to theoretical studies of fibrous filters.

Inertial fibrous filters offer a promising alternative to low-pressure impactors for nanoparticle sampling. They operate at high flow rates and relatively low pressure drop, and therefore can provide a rapid collection of nanoparticle samples and minimize evaporation losses of semivolatile components in the captured particles. These advantages over low-pressure impactors deserve further exploration.

Filters composed of nanofibers have potential to become efficient and economical devices for removing nanoparticles from gas streams. But experiments indicate that such filters have lower quality factor for very small particles, which tends to be interpreted as being a concern about their competitiveness. It should be noted that the use of quality factor for performance

comparison is not appropriate. Without taking the price of energy into account, quality factor is not a cost-based indicator. In addition, nanofiber filters with a substantially lower mass, and hence lower material cost, can achieve the same level of collection efficiency as commercial filters. A systematic study of particle loading and clever design of stacking up nanofiber and microfiber mats would undoubtedly improve the usefulness of nanofiber filters.

APPENDIX

For the slip flow regime, Pich[11] suggested the following expression for the stream function based on the Kuwabara model for a filter fiber:

$$\psi = \frac{d_f U_0 \sin\theta\left[\frac{1}{r} - r + 2\left(1 + \frac{4\xi}{d_f}\right) r \ln r\right]}{\frac{8\xi}{d_f}\left(-\frac{1}{2} - \ln\alpha\right) - 2\ln\alpha - 3} \quad \text{(A1)}$$

where r is the dimensionless radial coordinate, θ is the angular coordinate, and ξ is the coefficient of slip (= 0.998λ for diffuse reflection). Eq A1 is valid for $Kn_f < 0.25$, $\alpha \ll 1$, and $(r-1) \ll 1$. The expression reduces to a simplified form of Kuwabara's solution when Kn_f and ξ approach zero.

Using a different set of boundary conditions, Yeh[12] obtained the following expression:

$$\psi = \frac{d_f U_0 \sin\theta\left[\frac{A_1}{r} + A_2 r + 2r\ln r - \frac{\alpha r^3}{2}\right]}{-2\ln\alpha + \frac{4\alpha - 3}{1 + Kn_f} + \frac{Kn_f(2\alpha - 1)^2}{1 + Kn_f} - \alpha^2} \quad \text{(A2)}$$

where A_1 and A_2 are given by:

$$A_1 = \frac{\left(1 - \frac{\alpha}{2}\right)(1 - Kn_f) + Kn_f\alpha}{1 + Kn_f} \quad \text{(A3)}$$

$$A_2 = \frac{(1-\alpha)(Kn_f - 1)}{1 + Kn_f} \quad \text{(A4)}$$

Eq A2 reduces to the Kuwabara solution when Kn_f approaches zero.

Symbols and Acronyms

A_F = area of filter presented to the aerosol flow
A_1, A_2 = functions of α and Kn_f defined in eqs A3 and A4
B = particle mobility
C = slip correction factor
CNC = condensation nuclei counter
CPC = condensation particle counter
d_f = fiber diameter
d_F = filter diameter
d_p = particle diameter
d_s = screen diameter
d_t = tube inner diameter
D = particle diffusion coefficient
DEHS = diethylhexyl sebacate
DMA = differential mobility analyzer
e = charge of an electron
e-PTFE = expanded polytetrafluoroethylene
E = collection efficiency
E_{ad} = adhesion energy
HEPA filter = high-efficiency particulate air filter
k = Boltzmann's constant
K_C = parameter for deposition due to Coulombic force
K_{In} = parameter for deposition due to dielectrophoretic force
K_p, K_s = mechanical constants for particle and surface material
$Ka = (1 - \alpha)/Ku$
Kn_f, Kn_p = fiber and particle Knudsen numbers
Ku = Kuwabara hydrodynamic factor
L = filter thickness
m = particle mass
MPPS = most penetrating particle size
MWCNT = multiwalled carbon nanotube
n_p = number of elementary charges on a particle
N, N_0 = number concentrations of aerosol particles leaving and entering filter
Pe = Peclet number
PSL = polystyrene latex
Q = flow rate
r = dimensionless radial coordinate (= $2\rho/d_f$)
R = interception parameter
R_C = critical value of interception parameter
Re_f, Re_p = fiber and particle Reynolds numbers
Stk = Stokes number
T = temperature
THAB = tetraheptyl ammonium bromide
U = flow velocity in a filter
U_p = particle velocity relative to the gas flow
U_0 = face velocity of filter
ULPA filter = ultra-low-penetration air filter
V_{cr} = critical velocity for thermal rebound
α = packing density of filter
Δp = pressure drop across a filter
ε_f, ε_p = dielectric constants of fiber and particle
ε_0 = permittivity of vacuum
η = single fiber efficiency
$\bar{\eta}_{CR}$ = average single fiber efficiency due to Coulombic force and interception acting together
η_D = single fiber efficiency due to convective Brownian diffusion
η_{DR} = single fiber efficiency due to the simultaneous action of convective Brownian diffusion and interception
η_I = single fiber efficiency due to inertial impaction
η_{In} = single fiber efficiency due to dielectrophoretic force
η_R = single fiber efficiency due to interception
λ = mean free path of gas molecules
μ = viscosity
ν = kinematic viscosity
ρ, θ = polar coordinates
ρ_p, ρ_g = particle and gas density
$\bar{\sigma}$ = average charge density on fiber surface
$\sigma_{p,s}$ = specific adhesion energy at interfacial contact area
ξ = coefficient of slip
ψ = stream function

AUTHOR INFORMATION

Corresponding Author

*E-mail: cswang@ntu.edu.tw.

Notes

The authors declare no competing financial interest.

REFERENCES

(1) Borm, P. J. A.; Kreyling, W. Toxicological Hazards of Inhaled Nanoparticles—Potential Implications for Drug Delivery. *J. Nanosci. Nanotechnol.* **2004**, *4*, 521.

(2) Kreyling, W. G.; Semmler, M.; Möller, W. Dosimetry and Toxicology of Ultrafine Particles. *J. Aerosol Med.* **2004**, *17*, 140.
(3) Mills, N. L.; Donaldson, K.; Hadoke, P. W.; Boon, N. A.; MacNee, W.; Cassee, F. R.; Sandström, T.; Blomberg, A.; Newby, D. E. Adverse Cardiovascular Effects of Air Pollution. *Nat. Clin. Pract. Cardiovasc. Med.* **2009**, *6*, 36.
(4) Oberdörster, G. Safety Assessment for Nanotechnology and Nanomedicine: Concepts of Nanotoxicology. *J. Intern. Med.* **2010**, *267*, 89.
(5) Davies, C. N. *Air Filtration*; Academic Press: London, 1973.
(6) Brown, R. C. *Air Filtration: An Integrated Approach to the Theory and Applications of Fibrous Filters*; Pergamon: Oxford, U.K., 1993.
(7) Lee, K. W.; Ramamurthi, M., Filter Collection. In *Aerosol Measurement: Principles, Techniques, and Applications*; Willeke, K., Baron, P. A., Eds.; Van Nostrand Reinhold: New York, 1993; p 179.
(8) Hinds, W. C. *Aerosol Technology: Properties, Behavior, and Measurement of Airborne Particles*, 2nd ed.; John Wiley & Sons: New York, 1999.
(9) Wang, C.-S. Electrostatic Forces in Fibrous Filters: a Review. *Powder Technol.* **2001**, *118*, 166.
(10) Kuwabara, S. The Forces Experienced by Randomly Distributed Parallel Circular Cylinders or Spheres in a Viscous Flow at Small Reynolds Numbers. *J. Phys. Soc. Jpn.* **1959**, *14*, 527.
(11) Pich, J., Theory of Aerosol Filtration by Fibrous and Membrane Filters. In *Aerosol Science*; Davies, C. N., Ed.; Academic Press: London, 1966; p 229.
(12) Yeh, H. C. Fundamental Study of Aerosol Filtration by Fibrous Filters. PhD thesis, University of Minnesota, Minneapolis, 1972.
(13) Kim, J. H.; Mulholland, G. W.; Kukuck, S. R.; Pui, D. Y. H. Slip Correction Measurements of Certified PSL Nanoparticles Using a Nanometer Differential Mobility Analyzer (Nano-DMA) for Knudsen Number From 0.5 to 83. *J. Res. Natl. Inst. Stand. Technol.* **2005**, *110*, 31.
(14) Stechkina, I. B.; Kirsch, A. A.; Fuchs, N. A. Studies on Fibrous Aerosol Filters—IV Calculation of Aerosol Deposition in Model Filters in the Range of Maximum Penetration. *Ann. Occup. Hyg.* **1969**, *12*, 1.
(15) Lee, K. W.; Liu, B. Y. H. Theoretical Study of Aerosol Filtration by Fibrous Filters. *Aerosol Sci. Technol.* **1982**, *1*, 147.
(16) Lall, A. A.; Seipenbusch, M.; Rong, W.; Friedlander, S. K. On-Line Measurement of Ultrafine Aggregate Surface Area and Volume Distributions by Electrical Mobility Analysis: II. Comparison of Measurements and Theory. *J. Aerosol Sci.* **2006**, *37*, 272.
(17) Fuchs, N. A. *The Mechanics of Aerosols*; Pergamon: Oxford, 1964.
(18) Wang, C.-S.; Friedlander, S. K. Determination of Surface Area and Volume of Nanoparticle Aggregates Deposited in the Human Respiratory Tract Using DMA Data. *J. Aerosol Sci.* **2007**, *38*, 980.
(19) Wang, J.; Chen, D. R.; Pui, D. Y. H. Modeling of Filtration Efficiency of Nanoparticles in Standard Filter Media. *J. Nanopart. Res.* **2007**, *9*, 109.
(20) Japuntich, D. A.; Franklin, L. M.; Pui, D. Y.; Kuehn, T. H.; Kim, S. C.; Viner, A. S. A Comparison of Two Nano-Sized Particle Air Filtration Tests in the Diameter Range of 10 to 400 Nanometers. *J. Nanopart. Res.* **2007**, *9*, 93.
(21) Kim, S. C.; Harrington, M. S.; Pui, D. Y. H. Experimental Study of Nanoparticles Penetration Through Commercial Filter Media. *J. Nanopart. Res.* **2007**, *9*, 117.
(22) Yamada, S.; Seto, T.; Otani, Y. Influence of Filter Inhomogeneity on Air Filtration of Nanoparticles. *Aerosol Air Qual. Res.* **2011**, *11*, 155.
(23) Stechkina, I. B.; Fuchs, N. A. Studies on Fibrous Aerosol Filters—I. Calculation of Diffusional Deposition of Aerosols in Fibrous Filters. *Ann. Occup. Hyg.* **1966**, *9*, 59.
(24) Payet, S. Filtration Stationnaire et Dynamique des Aérosols Liquides Submicroniques. Thèse de l'Université Paris XII, 1991.
(25) Payet, S.; Boulaud, D.; Madelaine, G.; Renoux, A. Penetration and Pressure Drop of a HEPA Filter During Loading with Submicron Liquid Particles. *J. Aerosol Sci.* **1992**, *23*, 723.
(26) Brown, R. C. Capture of Dust Particles in Filters by Line-Dipole Charged Fibres. *J. Aerosol Sci.* **1981**, *12*, 349.
(27) Pich, J.; Emi, H.; Kanaoka, C. Coulombic Deposition Mechanism in Electret Filters. *J. Aerosol Sci.* **1987**, *18*, 29.
(28) Otani, Y.; Emi, H.; Mori, J. Initial Collection Efficiency of Electret Filter and Its Durability for Solid and Liquid Particles. *KONA* **1993**, *11*, 207.
(29) Davies, C. N. The Separation of Airborne Dust and Particles. *Proc. Inst. Mech. Eng. (London)* **1952**, *B1*, 185.
(30) Werner, R. M.; Clarenburg, L. A. Aerosol Filters. Pressure Drop across Single-Component Glass Fiber Filters. *Ind. Eng. Chem. Process Des. Dev.* **1965**, *4*, 288.
(31) Pich, J. Pressure Drop of Fibrous Filters at Small Knudsen Numbers. *Ann. Occup. Hyg.* **1966**, *9*, 23.
(32) Wang, H.-C.; Kasper, G. Filtration Efficiency of Nanometer-Size Aerosol Particles. *J. Aerosol Sci.* **1991**, *22*, 31.
(33) Bradley, R. S. The Cohesive Force between Solid Surfaces and the Surface Energy of Solids. *Philos. Mag.* **1932**, *13*, 853.
(34) Hamaker, H. C. The London—van der Waals Attraction between Spherical Particles. *Physica* **1937**, *4*, 1058.
(35) Johnson, K. L.; Kendall, K.; Roberts, A. D. Surface Energy and the Contact of Elastic Solids. *Proc. R. Soc. London A* **1971**, *324*, 301.
(36) Johnson, K. L. Adhesion and Friction between a Smooth Elastic Spherical Asperity and a Plane Surface. *Proc. R. Soc. London A* **1997**, *453*, 163.
(37) Mouret, G.; Chazelet, S.; Thomas, D.; Bemer, D. Discussion About the Thermal Rebound of Nanoparticles. *Sep. Purif. Technol.* **2011**, *78*, 125.
(38) Otani, Y.; Emi, H.; Cho, S.-J.; Namiki, N. Generation of Nanometer Size Particles and Their Removal from Air. *Adv. Powder Technol.* **1995**, *6*, 271.
(39) Ichitsubo, H.; Hashimoto, T.; Alonso, M.; Kousaka, Y. Penetration of Ultrafine Particles and Ion Clusters Through Wire Screens. *Aerosol Sci. Technol.* **1996**, *24*, 119.
(40) Alonso, M.; Kousaka, Y.; Hashimoto, T.; Hashimoto, N. Penetration of Nanometer-Sized Aerosol Particles Through Wire Screen and Laminar Flow Tube. *Aerosol Sci. Technol.* **1997**, *27*, 471.
(41) Heim, M.; Mullins, B. J.; Wild, M.; Meyer, J.; Kasper, G. Filtration Efficiency of Aerosol Particles Below 20 Nanometers. *Aerosol Sci. Technol.* **2005**, *39*, 782.
(42) Kim, C. S.; Bao, L.; Okuyama, K.; Shimada, M.; Niinuma, H. Filtration Efficiency of a Fibrous Filter for Nanoparticles. *J. Nanopart. Res.* **2006**, *8*, 215.
(43) Huang, S.-H.; Chen, C.-W.; Chang, C.-P.; Lai, C.-Y.; Chen, C.-C. Penetration of 4.5 nm to 10 μm Aerosol Particles Through Fibrous Filters. *J. Aerosol Sci.* **2007**, *38*, 719.
(44) Shin, W. G.; Mulholland, G. W.; Kim, S. C.; Pui, D. Y. H. Experimental Study of Filtration Efficiency of Nanoparticles Below 20 nm at Elevated Temperatures. *J. Aerosol Sci.* **2008**, *39*, 488.
(45) Heim, M.; Attoui, M.; Kasper, G. The Efficiency of Diffusional Particle Collection onto Wire Grids in the Mobility Equivalent Size Range of 1.2—8 nm. *J. Aerosol Sci.* **2010**, *41*, 207.
(46) Sato, S.; Chen, D.-R.; Pui, D. Y. H. Molecular Dynamics Study of Nanoparticle Collision with a Surface—Implication to Nanoparticle Filtration. *Aerosol Air Qual. Res.* **2007**, *7*, 278.
(47) Jung, S.-c.; Suh, D.; Yoon, W.-s. Molecular Dynamics Simulation on the Energy Exchanges and Adhesion Probability of a Nano-Sized Particle Colliding with a Weakly Attractive Static Surface. *J. Aerosol Sci.* **2010**, *41*, 745.
(48) Boskovic, L.; Altman, I. S.; Agranovski, I. E.; Braddock, R. D.; Myojo, T.; Choi, M. Influence of Particle Shape on Filtration Processes. *Aerosol Sci. Technol.* **2005**, *39*, 1184.
(49) Boskovic, L.; Agranovski, I. E.; Braddock, R. D. Filtration of Nanosized Particles with Different Shape on Oil Coated Fibres. *J. Aerosol Sci.* **2007**, *38*, 1220.
(50) Boskovic, L.; Agranovski, I. E.; Altman, I. S.; Braddock, R. D. Filter Efficiency as a Function of Nanoparticle Velocity and Shape. *J. Aerosol Sci.* **2008**, *39*, 635.

(51) Kim, S. C.; Wang, J.; Emery, M. S.; Shin, W. G.; Mulholland, G. W.; Pui, D. Y. H. Structural Property Effect of Nanoparticle Agglomerates on Particle Penetration Through Fibrous Filter. *Aerosol Sci. Technol.* **2009**, *43*, 344.
(52) Seto, T.; Furukawa, T.; Otani, Y.; Uchida, K.; Endo, S. Filtration of Multi-Walled Carbon Nanotube Aerosol by Fibrous Filters. *Aerosol Sci. Technol.* **2010**, *44*, 734.
(53) Hubbard, J. A.; Brockmann, J. E.; Dellinger, J.; Lucero, D. A.; Sanchez, A. L.; Servantes, B. L. Fibrous Filter Efficiency and Pressure Drop in the Viscous-Inertial Transition Flow Regime. *Aerosol Sci. Technol.* **2012**, *46*, 138.
(54) Robinson, M.; Franklin, H. The Pressure Drop of a Fibrous Filter at Reduced Ambient Pressures. *J. Aerosol Sci.* **1972**, *3*, 413.
(55) Otani, Y.; Eryu, K.; Furuuchi, M.; Tajima, N.; Tekasakul, P. Inertial Classification of Nanoparticles with Fibrous Filters. *Aerosol Air Qual. Res.* **2007**, *7*, 343.
(56) Furuuchi, M.; Eryu, K.; Nagura, M.; Hata, M.; Kato, T.; Tajima, N.; Sekiguchi, K.; Ehara, K.; Seto, T.; Otani, Y. Development and Performance Evaluation of Air Sampler with Inertial Filter for Nanoparticle Sampling. *Aerosol Air Qual. Res.* **2010**, *10*, 185.
(57) Kim, K. H.; Sekiguchi, K.; Kudo, S.; Sakamoto, K.; Hata, M.; Furuuchi, M.; Otani, Y.; Tajima, N. Performance Test of an Inertial Fibrous Filter for Ultrafine Particle Collection and the Possible Sulfate Loss when Using an Aluminum Substrate with Ultrasonic Extraction of Ionic Compounds. *Aerosol Air Qual. Res.* **2010**, *10*, 616.
(58) Miguel, A. F. Effect of Air Humidity on the Evolution of Permeability and Performance of a Fibrous Filter During Loading with Hygroscopic and Non-Hygroscopic Particles. *J. Aerosol Sci.* **2003**, *34*, 783.
(59) Podgórski, A.; Bałazy, A.; Gradoń, L. Application of Nanofibers to Improve the Filtration Efficiency of the Most Penetrating Aerosol Particles in Fibrous Filters. *Chem. Eng. Sci.* **2006**, *61*, 6804.
(60) Yun, K. M.; Hogan, C. J., Jr.; Matsubayashi, Y.; Kawabe, M.; Iskandar, F.; Okuyama, K. Nanoparticle Filtration by Electrospun Polymer Fibers. *Chem. Eng. Sci.* **2007**, *62*, 4751.
(61) Wang, J.; Kim, S. C.; Pui, D. Y. H. Investigation of the Figure of Merit for Filters with a Single Nanofiber Layer on a Substrate. *J. Aerosol Sci.* **2008**, *39*, 323.
(62) Leung, W. W.-F.; Hung, C.-H.; Yuen, P.-T. Effect of Face Velocity, Nanofiber Packing Density and Thickness on Filtration Performance of Filters with Nanofibers Coated on a Substrate. *Sep. Purif. Technol.* **2010**, *71*, 30.
(63) Hung, C.-H.; Leung, W. W.-F. Filtration of Nano-Aerosol Using Nanofiber Filter under Low Peclet Number and Transitional Flow Regime. *Sep. Purif. Technol.* **2011**, *79*, 34.
(64) Park, J. H.; Yoon, K. Y.; Na, H.; Kim, Y. S.; Hwang, J.; Kim, J.; Yoon, Y. H. Fabrication of a Multi-Walled Carbon Nanotube-Deposited Glass Fiber Air Filter for the Enhancement of Nano and Submicron Aerosol Particle Filtration and Additional Antibacterial Efficacy. *Sci. Total Environ.* **2011**, *409*, 4132.
(65) Tien, C.; Wang, C.-S.; Barot, D. T. Chainlike Formation of Particle Deposits in Fluid-Particle Separation. *Science* **1977**, *196*, 983.
(66) Kanaoka, C.; Emi, H.; Hiragi, S.; Myojo, T. Morphology of Particulate Agglomerates on a Cylindrical Fiber and Collection Efficiency of a Dust-Loaded Filter. In *Aerosols—Formation and Reactivity (Proceedings of the Second International Aerosol Conference), Berlin*; Pergamon Press: Oxford, 1986; p 674.
(67) Kasper, G.; Schollmeier, S.; Meyer, J. Structure and Density of Deposits Formed on Filter Fibers by Inertial Particle Deposition and Bounce. *J. Aerosol Sci.* **2010**, *41*, 1167.
(68) Schmidt, E. Simulation of Three-Dimensional Dust Structures via Particle Trajectory Calculations for Cake-Forming Filtration. *Powder Technol.* **1996**, *86*, 113.
(69) Endo, Y.; Chen, D.-R.; Pui, D. Y. H. Effects of Particle Polydispersity and Shape Factor During Dust Cake Loading on Air Filters. *Powder Technol.* **1998**, *98*, 241.
(70) Thomas, D.; Contal, P.; Renaudin, V.; Penicot, P.; Leclerc, D.; Vendel, J. Modelling Pressure Drop in HEPA Filters During Dynamic Filtration. *J. Aerosol Sci.* **1999**, *30*, 235.
(71) Brown, R. C.; Wake, D. Loading Filters with Monodisperse Aerosols: Macroscopic Treatment. *J. Aerosol Sci.* **1999**, *30*, 227.
(72) Sakano, T.; Otani, Y.; Namiki, N.; Emi, H. Particle Collection of Medium Performance Air Filters Consisting of Binary Fibers Under Dust Loaded Conditions. *Sep. Purif. Technol.* **2000**, *19*, 145.
(73) Kanaoka, C.; Hiragi, S.; Tanthapanichakoon, W. Stochastic Simulation of the Agglomerative Deposition Process of Aerosol Particles on an Electret Fiber. *Powder Technol.* **2001**, *118*, 97.
(74) Ji, J. H.; Bae, G. N.; Kang, S. H.; Hwang, J. Effect of Particle Loading on the Collection Performance of an Electret Cabin Air Filter for Submicron Aerosols. *J. Aerosol Sci.* **2003**, *34*, 1493.
(75) Tanthapanichakoon, W.; Maneeintr, K.; Charinpanitkul, T.; Kanaoka, C. Estimation of Collection Efficiency Enhancement Factor for an Electret Fiber with Dust Load. *J. Aerosol Sci.* **2003**, *34*, 1505.
(76) Song, C. B.; Park, H. S.; Lee, K. W. Experimental Study of Filter Clogging with Monodisperse PSL Particles. *Powder Technol.* **2006**, *163*, 152.
(77) Sae-lim, W.; Tanthapanichakoon, W.; Kanaoka, C. Correlation for the Efficiency Enhancement Factor of a Single Electret Fiber. *J. Aerosol Sci.* **2006**, *37*, 228.
(78) Kim, S. C.; Wang, J.; Shin, W. G.; Scheckman, J. H.; Pui, D. Y. H. Structural Properties and Filter Loading Characteristics of Soot Agglomerates. *Aerosol Sci. Technol.* **2009**, *43*, 1033.
(79) Kasper, G.; Schollmeier, S.; Meyer, J.; Hoferer, J. The Collection Efficiency of a Particle-Loaded Single Filter Fiber. *J. Aerosol Sci.* **2009**, *40*, 993.
(80) Leung, W. W.-F.; Hung, C.-H. Investigation on Pressure Drop Evolution of Fibrous Filter Operating in Aerodynamic Slip Regime under Continuous Loading of Sub-Micron Aerosols. *Sep. Purif. Technol.* **2008**, *63*, 691.
(81) Leung, W. W.-F.; Hung, C.-H.; Yuen, P.-T. Experimental Investigation on Continuous Filtration of Sub-Micron Aerosol by Filter Composed of Dual-Layers Including a Nanofiber Layer. *Aerosol Sci. Technol.* **2009**, *43*, 1174.
(82) Przekop, R.; Gradoń, L. Deposition and Filtration of Nanoparticles in the Composites of Nano- and Microsized Fibers. *Aerosol Sci. Technol.* **2008**, *42*, 483.
(83) Hosseini, S. A.; Vahedi Tafreshi, H. Modeling Particle Filtration in Disordered 2-D Domains: A Comparison with Cell Models. *Sep. Purif. Technol.* **2010**, *74*, 160.
(84) Hosseini, S. A.; Vahedi Tafreshi, H. 3-D Simulation of Particle Filtration in Electrospun Nanofibrous Filters. *Powder Technol.* **2010**, *201*, 153.